with the possible boundary types being determined by the constraint that vacancies never exist as nearest neighbours along the tunnels (Mijlhoff *et al.*, 1985; Kesson & White, 1986*a*). Further experiments are being carried out to investigate the effect of annealing on the growth of these domains.

We wish to acknowledge the support given to this work by the Australian Nuclear Science and Technology Organization (Research Contract No. 82/X/1) and the Australian Institute of Nuclear Science and Engineering.

References

BURSILL, L. A. & GRZINIC, G. (1980). *Acta Cryst.* B**36**, 2902–2913.
BYSTRÖM, A. & BYSTRÖM, A. M. (1950). *Acta Cryst.* **3**, 146–154.
CADEE, M. C. & VERSCHOOR, G. C. (1978). *Acta Cryst.* B**34**, 3554–3558.
CHEARY, R. W. (1986). *Acta Cryst.* B**42**, 229–236.
CHEARY, R. W. (1987). *Acta Cryst.* B**43**, 28–34.
CHEARY, R. W., HUNT, J. V. & CALAIZIS, P. (1981). *J. Aust. Ceram. Soc.* **17**, 11–12.
DRYDEN, J. C. & WADSLEY, A. D. (1958). *Trans. Faraday Soc.* **54**, 1574–1580.
FANCHON, E., VICAT, J., HODEAU, J. L., WOLFERS, P., TRAN QUI, D. & STROBEL, P. (1987). *Acta Cryst.* B**43**, 440–448.
HOWARD, C. J. (1982). *J. Appl. Cryst.* **15**, 615–620.
HOWARD, C. J., BALL, C. J., DAVIS, L. D. & ELCOMBE, M. M. (1983). *Aust. J. Phys.* **35**, 507–518.
HOWARD, C. J. & HILL, R. J. (1986). Australian Atomic Energy Commission Report, Lucas Height Research Laboratories. AAEC/M112.
KESSON, S. E. (1983). *Radioact. Waste Manage.* **4**, 53–72.
KESSON, S. E. & WHITE, T. J. (1986*a*). *Proc. R. Soc. London Ser. A*, **405**, 73–101.
KESSON, S. E. & WHITE, T. J. (1986*b*). *Proc. R. Soc. London Ser. A*, **408**, 295–319.
MIJLHOFF, F. C., IJDO, D. J. W. & ZANDERBERGEN, H. W. (1985). *Acta Cryst.* B**41**, 98–101.
POST, J. E., VON DREELE, R. B. & BUSECK, P. R. (1982). *Acta Cryst.* B**38**, 1056–1065.
ROTH, R. (1981). Annual Report, National Measurements Laboratory, Office of Nuclear Technology. NBSIR 81-2241.
WEBER, H. P. & SCHULTZ, H. (1986). *J. Chem. Phys.* **85**, 475–484.
WILES, D. B. & YOUNG, R. A. (1981). *J. Appl. Cryst.* **14**, 149–150.

Acta Cryst. (1989). B**45**, 212–218

Structure of ND_4F-II

BY A. C. LAWSON AND R. B. ROOF

Los Alamos National Laboratory, Los Alamos, New Mexico 87545, *USA*

J. D. JORGENSEN

Argonne National Laboratory, Argonne, Illinois 60439, *USA*

AND B. MOROSIN AND J. E. SCHIRBER

Sandia National Laboratories, Albuquerque, New Mexico 87185, *USA*

(*Received* 21 *July* 1988; *accepted* 3 *January* 1989)

Abstract

The crystal structure of ND_4F-II has been determined at 4·69 kbar ($4{\cdot}69 \times 10^5$ kPa) at room temperature [$a_{II} = 8{\cdot}508(1)$, $c_{II} = 16{\cdot}337(2)$ Å, $V = 1024{\cdot}1(2)$ Å^3, $R_{wp} = 2{\cdot}91\%$ for 250 reflections]. The structure is rhombohedral, space group $R3c$, with 24 molecules per hexagonal unit cell. Like its parent phase, ND_4F-I with the hexagonal wurtzite structure, it consists of corner-sharing tetrahedral units. However, it has a structure that is topologically distinct from that of the ND_4F-I phase and that accounts for the 28% volume collapse observed at the I–II transition. The transition is accomplished by filling the empty space in the parent structure, with reductions in the volumes of the tetrahedral units of only 2·4–5·2%. The ND_4F-II phase was found to be stable down to at least 50 K, and its thermal expansion was determined. The anisotropic compressibility of the ND_4F-I phase at room temperature is also reported.

Introduction

Under ordinary conditions of temperature and pressure NH_4F has the wurtzite structure (Zachariasen, 1927). It is useful to visualize this structure in terms of hexagonally close-packed layers of F atoms that give rise to a network of corner-sharing tetrahedra. The NH_4^+ ions fit nicely into alternate tetrahedra, and a nearly perfect tetrahedral arrangement of N–H–F hydrogen bonds is achieved (Adrian & Feil, 1969; Morosin, 1970). The resulting structure does not fill space very efficiently, as the fraction of space filled by

0108-7681/89/030212-07$03.00

the packed tetrahedra is only 1/6. This phase is known as NH_4F-I.*

Stevenson (1961) discovered that NH_4F-I undergoes a pressure-induced phase transformation at 3·8 kbar (1 kbar = 10^5 kPa) to a phase that has 28% less molar volume. This phase is known as NH_4F-II. The occurrence of this phase transition was subsequently confirmed by Swenson & Tedeschi (1964) who also determined that the transition pressure is nearly independent of temperature. Such a spectacular decrease in molar volume suggests a first-order transition involving a drastic change in crystal structure. However, the structure of NH_4F-II has not been determined until now despite at least three previous attempts. Morosin & Schirber (1965) obtained X-ray powder diffraction data at high pressure and suggested a tetragonal unit cell which explained their observed *d* spacings. Nabor, Calvert & Whalley (1969) obtained a more extensive set of X-ray powder diffraction *d* spacings and intensities on a sample that was pressure quenched at low temperature. These data were sufficiently complete to disprove the tetragonal cell of Morosin & Schirber but did not suggest a new model for the structure. Finally, Smith, Schirber & Morosin (1982) performed a preliminary high-pressure time-of-flight neutron diffraction experiment on a powder sample of ND_4F. Smith *et al.* generally confirmed the data of Nabor *et al.* (1969) and demonstrated the utility of the time-of-flight diffraction technique for this problem, but their data were not of sufficient quality to allow a determination of the structure.

Nabor *et al.* (1969) also discovered and named several other phases of NH_4F: NH_4F-V and NH_4F-VII are stacking variants of NH_4F-I, NH_4F-III has a structure related to that of CsCl, and the structure of NH_4F-VI is still unknown. Only NH_4F-I and NH_4F-II will be discussed further in this paper.

The crystallographic behavior of NH_4F differs from that of both the other ammonium halides and of the alkali halides (Megaw, 1973) because of the presence of strong hydrogen bonding between nitrogen and fluorine. The occurrence of these bonds results in a marked preference for tetrahedral coordination for the ammonium ion. The compound most similar to NH_4F-I is water – in the form of hexagonal ice-I (Pauling, 1960).

Experimental procedure

High-pressure neutron powder diffraction data were obtained of a sample of ND_4F using the 90° detector banks of the Special Environment Powder Diffractometer (SEPD). This instrument operates at the Intense Pulsed Neutron Source (IPNS) at Argonne National Laboratory. The diffractometer (Jorgensen & Faber, 1982) and the high-pressure technique (Worlton, Decker, Jorgensen & Kleb, 1986) have been previously described. The diffractometer was calibrated with a standard silicon sample, for which the lattice constant was taken to be 5·4307 Å. For powder diffraction work, the choice of a deuterated sample is dictated by the unfavorably high incoherent neutron-scattering cross section of the protium hydrogen isotope. The ND_4F sample was prepared by repeated recrystallization in D_2O. The high pressure was transmitted to the sample by means of helium gas, so that the pressure was always hydrostatic provided that the temperature did not fall below the freezing point of helium. Low temperatures were obtained by the use of a closed-cycle helium refrigerator. All sample handling procedures were carried out in a helium-filled glove-bag to prevent absorption of water by the extremely hygroscopic ND_4F powder; the importance of careful sample handling has been detailed by Swenson & Tedeschi (1964).

For use in subsequent Rietveld analysis, an effective incident neutron intensity *versus* wavelength spectrum valid down to *d* spacings of 0·8 Å was determined for the sample inside the high-pressure cell. This was accomplished by measuring the transmitted beam with a detector whose efficiency matches the detectors in the scattered flightpath. The method works because it avoids the multiple-scattering problems that would be present in any attempt to determine the incident spectrum by placing vanadium in the pressure cell.

Seven neutron powder diffraction data sets were collected using the time-of-flight method: two on ND_4F-I and five on ND_4F-II. For indexing purposes a preliminary analysis of the ND_4F-II data was made with the *TOFMANY* individual peak-fitting code (Faber & Hitterman, 1986). The data were further analyzed and refined using the Rietveld profile-analysis method as implemented in the *Generalized Crystal Structure Analysis System* (*GSAS*) (Larson & Von Dreele, 1986). The average for the *z* coordinates of all the atoms was held constant during the refinement. In the case of ND_4F-I, the origin was shifted to place the F atom at $z=0$. The thermal parameters were assumed to be isotropic and were constrained to be equal for all atoms of each element. Trial refinements using anisotropic thermal parameters did not produce significantly better results.

Experimental results

Stevenson (1961) and Swenson & Tedeschi (1964) both observed the transition at 3·8 kbar, while Morosin & Schirber observed it at 3·64 kbar. We observed a transition at room temperature at 4·69 (1) kbar, a pressure somewhat higher than that reported earlier.

* As explained in the subsequent text, deuterated ammonium fluoride was used for the experimental work described in this paper. We will use the formula NH_4F for non-isotope-specific references to the ammonium fluoride compound and reserve the formula ND_4F for specific references to the deuterated form.

The transition pressure of our neutron sample was subsequently redetermined on a second apparatus at Sandia, and good agreement was found with the results obtained at Argonne (4·76 kbar compared to 4·69 kbar.) The pressure calibration of the Sandia system was checked by measurement of the transition pressure of a sample of NH_4F. The transition pressure was within 2% of the result of the 1965 measurement in which the Heise gauge was standardized to a Harwood dead-weight gauge.

The lattice constants of our sample as determined by Rietveld analysis are at slight variance with those reported by Morosin & Schirber (1965). After the completion of the neutron measurements, we found that infrared spectra taken on our sample show the presence of unidentified impurities at the level of a few percent. These impurities were not detected in the neutron measurements, and we do not believe that they affect the structural results reported here. However, such a large elevation of the transition pressure by a few percent of impurities is surprising.

Two data sets were obtained on ND_4F-I at room temperature (300 K) in the pressure cell, at ambient pressure and 4·60 kbar (just *below* the transition). The ambient pressure data are shown in Figs. 1 and 2. These figures show the observations, the Rietveld fit to the wurtzite-structure model, and the difference between the observed and calculated profiles. The weighted-profile R value for this fit is 6·17%, and the reduced χ-squared value (the ratio of the observed R value to that expected on the basis of statistics) is 1·79. The fit for the 4·60 kbar data is of the same quality.

Four data sets were obtained on ND_4F-II at a constant pressure of 4·60 kbar and various temperatures between 300 and 50 K. Figs. 3 and 4 show the Rietveld fit to a model that will be described presently for the data obtained at 300 K and 4·69 kbar (just *above* the transition).* Again the fit is excellent. A seventh data set was obtained at 50 K upon the release

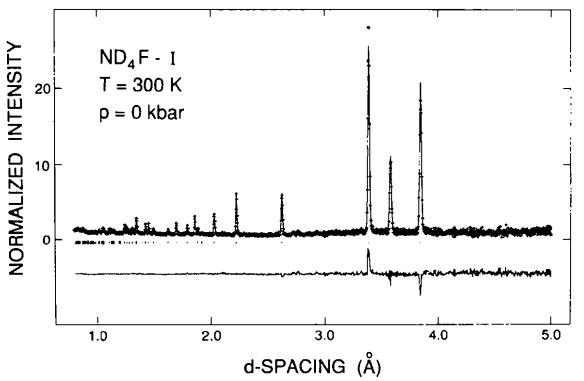

Fig. 1. Time-of-flight neutron powder diffraction data for ND_4F-I for $0{\cdot}8 < d < 5{\cdot}0$ Å. The crosses are the observed intensities normalized by the incident spectrum and the line is the Rietveld fit. The small vertical bars indicate the positions of allowed *hkl* reflections. The difference between the observed and calculated profiles is plotted below the diffraction pattern. The data were taken on the Special Environment Powder Diffractometer (SEPD) at the Intense Pulsed Neutron Source (IPNS) at Argonne National Laboratory.

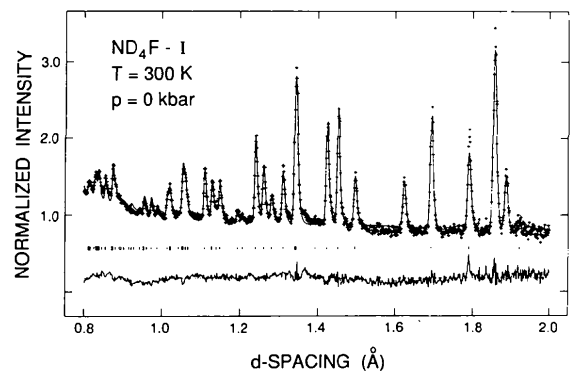

Fig. 2. Time-of-flight neutron powder diffraction data for ND_4F-I for $0{\cdot}8 < d < 2{\cdot}0$ Å. See caption of Fig. 1 for details.

* A list of numerical values corresponding to Figs. 1 and 2 has been deposited with the British Library Document Supply Centre as Supplementary Publication No. SUP 51552 (13 pp.). Copies may be obtained through The Executive Secretary, International Union of Crystallography, 5 Abbey Square, Chester CH1 2HU, England.

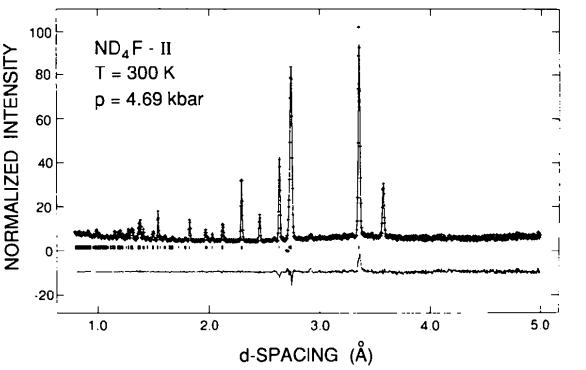

Fig. 3. Time-of-flight neutron powder diffraction data for ND_4F-II for $0{\cdot}8 < d < 5{\cdot}0$ Å. See caption of Fig. 1 for details.

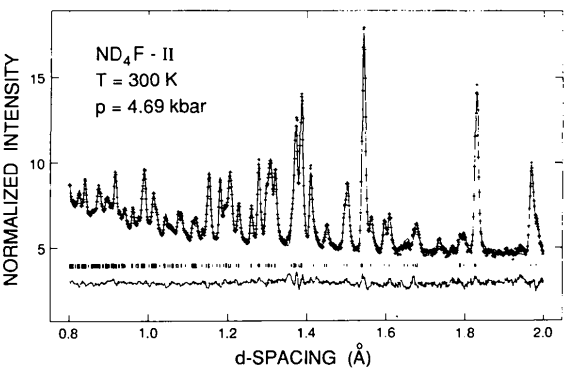

Fig. 4. Time-of-flight neutron powder diffraction data for ND_4F-II for $0{\cdot}8 < d < 2{\cdot}0$ Å. See caption of Fig. 1 for details.

Table 1. *Crystal data for* ND_4F-I

Pressure (kbar)			0		4·60 (1)	
Space group			$P6_3mc$		$P6_3mc$	
Lattice constants						
a_I (Å)			4·436 (1)		4·436 (1)	
c_I (Å)			7·158 (1)		7·090 (2)	
Cell volume (Å^3)			121·99 (4)		120·81 (5)	
Volume per formula unit (Å^3)			60·99 (2)		60·40 (3)	
Atomic positions						
	x	y	z	x	y	z
N(1)	$\frac{1}{3}$	$\frac{2}{3}$	0·3735 (3)	$\frac{1}{3}$	$\frac{2}{3}$	0·3758 (5)
F(1)	$\frac{1}{3}$	$\frac{2}{3}$	0·0000 (5)	$\frac{1}{3}$	$\frac{2}{3}$	0·0000 (8)
D(1)	$\frac{1}{3}$	$\frac{2}{3}$	0·2308 (5)	$\frac{1}{3}$	$\frac{2}{3}$	0·2329 (7)
D(2)	0·4583 (3)	−0·4583	0·4214 (4)	0·4572 (5)	−0·4572	0·4231 (6)
Isotropic U's						
U_N (Å^2)			0·026 (1)		0·024 (2)	
U_F (Å^2)			0·030 (2)		0·031 (3)	
U_D (Å^2)			0·040 (1)		0·040 (2)	
Weighted profile R (%)			6·17		9·46	
Reduced χ-squared			1·79		1·28	
No. of variables			24		24	

Table 2. *Bond lengths* (Å) *and angles* (°) *for* ND_4F-I

	0 kbar	4·60 kbar
Tetrahedral lengths		
F(1*a*)–F(1*b*)	4·401 (1)	4·373 (2)
F(1*a*)–F(1*b*)	4·436 (1)	4·436 (3)
Tetrahedral angles		
F(1*a*)–F(1*b*)–F(1*b*)	59·74 (1)	59·52 (2)
F(1*b*)–F(1*a*)–F(1*b*)	60	60
Tetrahedral volume (Å^3)	10·166 (5)	10·067 (5)
Chemical lengths (Å)		
N–F(1*a*)	2·672 (7)	2·666 (10)
N–F(1*b*)	2·717 (2)	2·707 (4)
N–D(1)	1·025 (5)	1·020 (7)
N–D(2)	1·025 (3)	1·018 (5)
D1–F(1*a*)	1·647 (7)	1·647 (11)
D2–F(1*b*)	1·692 (4)	1·690 (6)
Chemical angles (°)		
D(2)–N–D(2)	108·8 (8)	109·6 (4)
D(1)–N–D(2)	110·5 (5)	109·6 (4)
N–D(1)–F(1*a*)	180	180
N–D(2)–F(1*b*)	179·758 (1)	179·294 (6)

of pressure. The data showed that the ND_4F-II structure was maintained upon the release of pressure at low temperature, just as observed by Nabor *et al.* (1969). Upon warming to room temperature, however, the sample transformed back to the ND_4F-I structure.

Description of the structures

We confirmed the wurtzite structure for ND_4F-I, with $a_I = 4{\cdot}436$ (1) and $c_I = 7{\cdot}158$ (1) Å. [Morosin & Schirber observed $a_I = 4{\cdot}4378$ (4) and $c_I = 7{\cdot}1635$ (4) Å.] Structural data for this phase are given in Table 4 for both 0 and 4·60 kbar at 300 K. The derived bond lengths and angles are given in Table 2. [The total number of refined variables exceeds the number given in Tables 1 and 3 because it is necessary to refine certain 'instrumental' variables (*e.g.*, scale factors, background and peak-width parameters) that are of no structural interest.]

Table 2 gives two types of data: 'tetrahedral' and 'chemical.' Tetrahedral lengths and angles refer to the size and shape of the corner-sharing fluorine tetrahedra and have geometrical significance only. Chemical lengths and angles describe the bonding of atoms within each tetrahedron. Fig. 5 shows the layers of tetrahedra which constitute the structure, and Fig. 6 shows two tetrahedra of the structure in detail and provides a key to Table 2. The structural data cannot be compared directly with those of Adrian & Feil (1969) because their study was performed at 77 K; however, the agreement with their results seems reasonable. For our sample, the compressibility of the ND_4F-I phase is anisotropic with nearly all of the compression along the crystallographic c axis. As explained earlier, this discrepancy with earlier measurements (Morosin, 1970) may be the result of impurities.

We found that ND_4F-II crystallizes in the non-centrosymmetric group $R3c$, with 24 molecules per hexagonal unit cell. The unit cell is large, with $a_{II} = 8{\cdot}508$ (1) and $c_{II} = 16{\cdot}337$ (2) Å. Although the correspondences $2a_I \rightarrow a_{II}$ and $3c_I \rightarrow c_{II}$ hold between the lattice constants of the two phases, the 28% volume collapse is accomplished with compression almost entirely along the c axis. Hence, the structure is

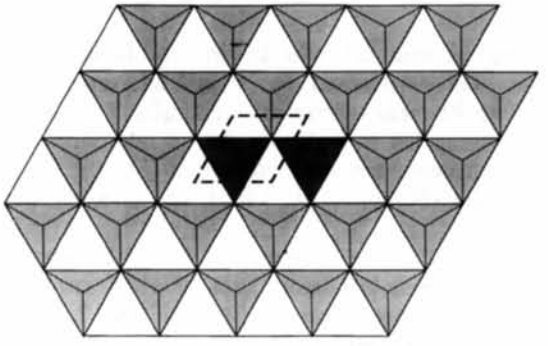

Fig. 5. (0001)-Projection of a single layer of the ND_4F-I structure. The dotted line indicates a unit cell, and the darker tetrahedra are shown in the next figure.

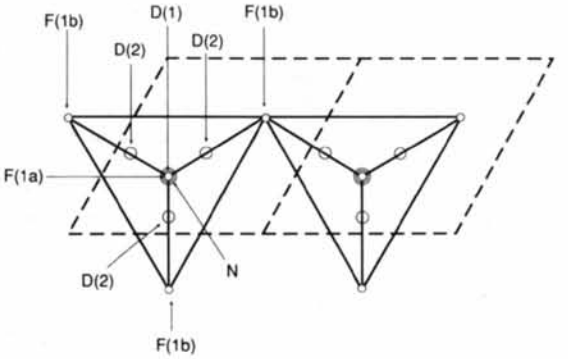

Fig. 6. Detail of the ND_4F-I structure in (0001)-projection. Two unit cells containing corner-linked tetrahedra are shown.

Table 3. *Crystal data for* ND_4F-II

Space group		$R3c$	
Lattice constants			
a_H (Å)		8·508 (1)	
c_H (Å)		16·337 (2)	
Cell volume (Å³)		1024·1 (2)	
Volume per formula unit (Å³)		42·672 (8)	
Atomic positions			
	x	y	z
N(1)	⅓	⅔	0·5738 (3)
N(2)	0·7013 (4)	0·7863 (4)	0·5143 (2)
F(1)	⅓	⅔	0·7512 (3)
F(2)	0·4521 (6)	0·4249 (8)	0·4934 (2)
D(1)	⅓	⅔	0·6362 (3)
D(2)	0·5777 (7)	0·3672 (6)	0·5517 (2)
D(3)	0·6425 (6)	0·8632 (6)	0·5137 (3)
D(4)	0·6130 (7)	0·6628 (8)	0·4992 (3)
D(5)	0·8155 (5)	0·8532 (6)	0·4744 (3)
D(6)	0·7444 (5)	0·7753 (6)	0·5699 (3)
Isotropic U's			
U_N (Å²)	0·0169 (5)		
U_F (Å²)	0·0092 (9)		
U_D (Å²)	0·0246 (7)		
Weighted profile R (%)	2·91		
Reduced χ-squared	2·45		
No. of variables	43		

completely reorganized and cannot be considered as a multicell of the ambient phase. Indeed, the structural significance of these metric relationships was recognized only after the structure of ND_4F-II was solved.

Once the unit cell was known, the location of the atoms was determined by a trial-and-error method using the Rietveld refinement technique. The structural details are given in Table 3. As an additional check, calculated intensities were compared with the available X-ray data (Nabor *et al.*, 1969), and good agreement was found.

Like ND_4F-I, the structure of ND_4F-II consists of layers of fluorine tetrahedra each of which contains an ND_4^+ ion. A single layer is shown in Fig. 7, and Fig. 8 shows the structure in detail. Two kinds of tetrahedra are present in each layer; one tetrahedron sits on a threefold axis and has that symmetry, while the other is nonsymmetric. The two tetrahedra occur in the structure in the ratio 1:3. A comparison of Figs. 5 and 7 shows that the main difference between the structure of the layers in the two phases is that a considerable orientational distortion exists in the ND_4F-II layers as compared with those of ND_4F-I. However, this distortion is accompanied by almost no change in the basal plane area per tetrahedron.

Three distinct structural features with threefold symmetry are found in the unit cell. One of these features (*A* in Fig. 7) is the axis of the threefold tetrahedron. The second (*B*) is a hole surrounded by edges of nonsymmetric tetrahedra. The third (*C*) is the vertex formed by the junction of three nonsymmetric tetrahedra. In three dimensions, these features are stacked alternately along the threefold axis.

The principal difference between the three-dimensional structures of NH_4F-I and NH_4F-II is the nature of the interlayer connection. In NH_4F-II, the nonsymmetric tetrahedra are connected by corner-shared fluorine atoms to layers directly above them, just as in ND_4F-I. However, the threefold tetrahedra are connected not to the layer directly above, but to the next higher layer, *via* the threefold hole in the intervening layer. This unusual connectivity is accompanied by a 30% decrease of the c lattice constant. Much more efficient use of space is achieved, while still allowing tetrahedral coordination of the ND_4^+ ions.

The tetrahedral lengths and angles for ND_4F-II are given in Table 4. The entries in this table do not represent chemical bonds, but rather show the geometrical deviation of the tetrahedra from the ideal. The distortion is extremely large for both types of tetrahedra but does not necessarily have chemical significance. In the high-pressure structure, the tetrahedral volumes are 2·4–5·2% smaller than that of ND_4F-I at 4·69 kbar (Table 2). This shows directly that

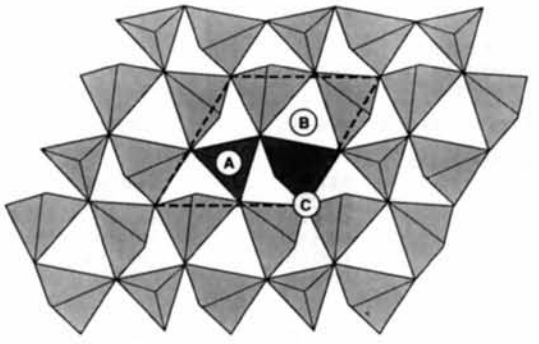

Fig. 7. (0001)-Projection of a single layer of the ND_4F-II structure. Two types of tetrahedra are present. *A*, *B* and *C* denote structural features with threefold symmetry. The dotted line indicates a unit cell, and the darker tetrahedra are shown in the next figure.

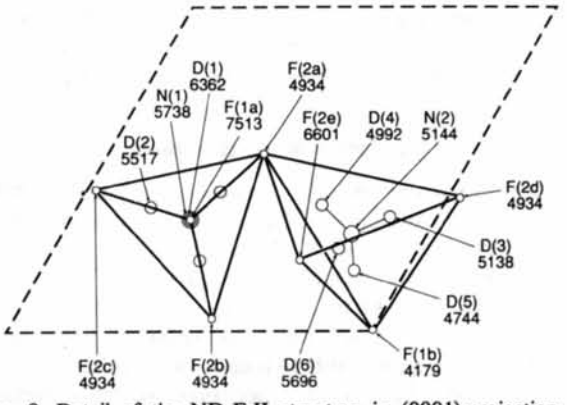

Fig. 8. Detail of the ND_4F-II structure in (0001)-projection. A single unit cell containing two corner-linked tetrahedra is shown. The numbers below the atom labels are the z coordinates of the atoms in units of $c/10\,000$.

Table 4. *Tetrahedral lengths* (Å) *and angles* (°) *for* ND_4F-II

Threefold tetrahedron			
F(1*a*)–F(2*a*)	4·807 (6)	F(1*a*)–F(2*a*)–F(2*b*)	65·35 (5)
F(2*a*)–F(2*b*)	4·010 (7)	F(2*a*)–F(1*a*)–F(2*b*)	49·31 (10)
		F(2*a*)–F(2*b*)–F(2*c*)	60
Volume (Å^3)	9·539		
Irregular tetrahedron			
F(1*b*)–F(2*a*)	4·938 (5)	F(2*a*)–F(2*e*)–F(1*b*)	71·73
F(1*b*)–F(2*d*)	3·935 (5)	F(2*e*)–F(1*b*)–F(2*a*)	46·45 (5)
F(1*b*)–F(2*e*)	4·584 (7)	F(1*b*)–F(2*a*)–F(2*e*)	61·82 (9)
F(2*a*)–F(2*d*)	4·690 (7)	F(2*d*)–F(2*e*)–F(1*b*)	49·06
F(2*a*)–F(2*e*)	3·769 (2)	F(2*e*)–F(1*b*)–F(2*d*)	69·29 (12)
F(2*d*)–F(2*e*)	4·872 (6)	F(1*b*)–F(2*d*)–F(2*e*)	61·65 (14)
		F(2*d*)–F(2*e*)–F(2*a*)	64·26
Volume (Å^3)	9·816	F(2*e*)–F(2*a*)–F(2*d*)	69·36 (16)
		F(2*a*)–F(2*d*)–F(2*e*)	46·38 (4)
		F(2*d*)–F(2*a*)–F(1*b*)	44·16
		F(2*a*)–F(1*b*)–F(2*d*)	62·62 (11)
		F(1*b*)–F(2*d*)–F(2*a*)	69·22 (12)

Table 5. *Chemical bond lengths* (Å) *and angles* (°) *for* ND_4F-II

Threefold tetrahedron			
N(1)–F(1)	2·899 (7)	N(1)–D(1)–F(1)	180
N(1)–F(2)	2·622 (5)	N(1)–D(2)–F(2)	166·4 (5)
N(1)–D(1)	1·019 (6)	D(2)–N(1)–D(2)	107·8 (4)
N(1)–D(2)	1·002 (4)	D(1)–N(1)–D(2)	111·1 (4)
D(1)–F(1)	1·880 (9)		
D(1)–F(2)	1·677 (6)		
Irregular tetrahedron			
N(2)–F(2*d*)	2·770 (6)	N(2)–D(3)–F(2*d*)	166·4 (4)
N(2)–F(2*a*)	2·748 (6)	N(2)–D(4)–F(2*a*)	168·0 (5)
N(2)–F(1*b*)	2·761 (5)	N(2)–D(5)–F(1*b*)	168·1 (5)
N(2)–F(2*e*)	2·713 (5)	N(2)–D(6)–F(2*e*)	164·5 (4)
N(2)–D(3)	1·003 (5)	D(3)–N(2)–D(4)	109·6 (4)
N(2)–D(4)	0·970 (6)	D(3)–N(2)–D(5)	105·3 (4)
N(2)–D(5)	1·068 (5)	D(3)–N(2)–D(6)	113·4 (5)
N(2)–D(6)	1·000 (5)	D(4)–N(2)–D(5)	115·2 (5)
D(3)–F(2*d*)	1·785 (7)	D(4)–N(2)–D(6)	104·5 (5)
D(4)–F(2*a*)	1·791 (6)	D(5)–N(2)–D(6)	109·0 (4)
D(5)–F(1*b*)	1·707 (6)		
D(6)–F(2*e*)	1·736 (6)		

most of the observed volume change at the transition is at the expense of empty space.

The chemical lengths and angles for ND_4F-II are given in Table 5. The coordination of the D atoms around their respective N atoms remains essentially tetrahedral despite the large geometric distortions. In comparison to ND_4F-I, the N–D bonds are about the same, the D–F bonds are about 5% longer, and the N–D–F angles are bent by a little over 10°. The net result of the bond bending is that the lengths of the N–D–F bonds in ND_4F-II are 0–3·7% longer than in ND_4F-I. The short N(2)–D(4) bond length of 0·970 Å is somewhat less than that usually encountered in ammonium compounds. This should not cast doubt on the correctness of the structure in view of the reasonable values obtained for the remaining distances.

Table 6 shows the lattice constants and thermal factors for ND_4F-II at various temperatures. The linear thermal-expansion coefficients were calculated from the data at 100 K and above. We obtained the values $\alpha_a = 22\ (5) \times 10^{-6}\ K^{-1}$ and $\alpha_c = 24\ (3) \times 10^{-6}\ K^{-1}$, so

Table 6. *Temperature dependence of lattice constants and thermal factors of* ND_4F-II

P (kbar)	T (K)	a_{11} (Å)	c_{11} (Å)	U_N (Å^2)	U_F (Å^2)	U_D (Å^2)
4·69	300	8·508 (8)	16·337 (2)	0·0169 (5)	0·0092 (9)	0·0247 (7)
4·69	200	8·486 (1)	16·293 (2)	0·0096 (5)	0·0063 (10)	0·0184 (7)
4·69	100	8·471 (1)	16·259 (2)	0·0049 (4)	0·0028 (9)	0·0138 (7)
4·69	50	8·469 (1)	16·246 (2)	0·0022 (5)	−0·0014 (8)	0·0103 (6)
0·0	50	8·508 (1)	16·297 (2)	0·0022 (4)	0·0011 (7)	0·0111 (6)

that the thermal expansion is isotropic within experimental error. The thermal factors were used to calculate a Debye temperature for each atom type under the crude assumption that each element can be treated independently. We obtained the values 386 (5), 392 (12) and 860 (12) K for the N, F and D atoms, respectively. Because of the limited d range (> 0·8 Å) and the primitive model used for the Debye temperatures, the numbers have a comparative significance only.

To summarize, our model for the structure of ND_4F-II has a novel type of tetrahedral packing which satisfactorily explains the 28% volume collapse observed at the I–II transition of ND_4F. The model exhibits reasonable values for the bond lengths, bond angles, thermal expansions and Debye temperatures.

We have greatly benefitted from conversations with Allen Larson, Robert Von Dreele, Jim Richardson, Phil Rudolph and Joyce Goldstone, and we thank them for their help. One of us (ACL) is especially grateful to James L. Smith for introducing him to this problem and sharing preliminary data. Susan Carlson deserves special thanks for her excellent work on the figures. The Intense Pulsed Neutron Source is operated as a National User Facility by the US Department of Energy Basic Energy Sciences – Materials Sciences, under contract No. W-31-109-ENG-38. One of the authors (JDJ) also acknowledges support from the same agency. Research at Sandia is performed under the auspices of the US Department of Energy under contract No. DE-AC04-76DP 00789. Research at Los Alamos is supported by the US Department of Energy.

References

ADRIAN, H. W. W. & FEIL, D. (1969). *Acta Cryst.* A25, 438–444.

FABER, J. JR & HITTERMAN, R. L. (1986). *Advances in X-Ray Analysis*, edited by C. S. BARRETT, J. B. COHEN, J. FABER JR, R. JENKINS, B. E. LEYDEN, J. C. RUSS & P. K. PREDECKI, Vol. 29, pp. 119–130. New York: Plenum Press.

JORGENSEN, J. D. & FABER, J. JR (1982). *Proceedings of ICANS* VI, Report 82-80, edited by J. M. CARPENTER, pp. 105–112. Argonne National Laboratory, Argonne, USA.

LARSON, A. C. & VON DREELE, R. B. (1986). Unclassified Report, LAUR 86-748. Los Alamos National Laboratory, Los Alamos, USA.

MEGAW, H. D. (1973). *Crystal Structures: A Working Approach*, pp. 502–507. Philadelphia: W. B. Saunders.

MOROSIN, B. (1970). *Acta Cryst.* B**26**, 1635–1637.
MOROSIN, B. & SCHIRBER, J. E. (1965). *J. Chem. Phys.* **42**, 1389–1390.
NABOR, M. A., CALVERT, L. D. & WHALLEY, E. (1969). *J. Chem. Phys.* **51**, 1353–1356.
PAULING, L. (1960). *The Nature of the Chemical Bond*, 3rd ed., p. 464. Ithaca: Cornell Univ. Press.
SMITH, J. L., SCHIRBER, J. E. & MOROSIN, B. (1982). Private communication.
STEVENSON, R. (1961). *J. Chem. Phys.* **34**, 346–347.
SWENSON, C. A. & TEDESCHI, J. R. (1964). *J. Chem. Phys.* **40**, 1141–1143.
WORLTON, T. G., DECKER, D. L., JORGENSEN, J. D. & KLEB, R. (1986). *Physica*, **136B**, 503–506. Also *Neutron Scattering*, edited by G. H. LANDER & R. A. ROBINSON, pp. 503–506. Amsterdam: North-Holland.
ZACHARIASEN, W. H. (1927). *Z. Phys. Chem.* (*Leipzig*), **127**, 218–224.

Acta Cryst. (1989). B**45**, 218–227

Crystal Symmetry and Coherent Twin Structure of Calcium Zirconate

BY VINAYAK P. DRAVID, C. M. SUNG, M. R. NOTIS AND C. E. LYMAN

Department of Materials Science and Engineering, Lehigh University, Bethlehem, Pennsylvania 18015, *USA*

(*Received* 5 *July* 1988; *accepted* 11 *January* 1989)

Abstract

$CaZrO_3$ has been investigated at room temperature using a variety of electron microscopy techniques. Conventional transmission electron microscopy and high-resolution transmission electron miscroscopy revealed a characteristic coherent twin structure in $CaZrO_3$. In order to interpret the occurrence of the twin structure and the associated crystallography, the cell parameters and space-group symmetry of $CaZrO_3$ have been determined independently using convergent-beam electron diffraction. The results are consistent with those previously obtained by neutron diffraction. Both the crystal symmetry and lattice-parameter data have been used to explain the details of the twin structure in $CaZrO_3$.

Introduction

$CaZrO_3$ is a member of the large family of ABO_3 perovskite compounds. An ideal perovskite structure contains one formula unit and has a primitive cubic unit cell as shown in Fig. 1. Considerable attention has been given to the symmetry aspects of ABO_3 compounds and their close relationship with many engineering properties of these materials.

Structural studies of ABO_3 compounds are usually hampered by the difficulty of growing defect-free large single crystals. Furthermore, several ABO_3 compounds go through displacive and/or disorder–order phase transitions during cooling giving rise to domain structures. Therefore, there have been continual refinements of the crystal structure data of several ABO_3 compounds. (Tanaka, Saito & Tsuzuki, 1982; Vegas, Vallet-Regi, Gonzalez-Calbet & Alario-Franco, 1986).

$CaZrO_3$, in particular, has been the focus of only a small number of investigations (see Table 1). The first major study of ABO_3 compounds was conducted by Megaw (1946). She deduced from her powder X-ray diffraction (XRD) results that $CaZrO_3$ possessed orthorhombic symmetry at room temperature with cell parameters $a = 1{\cdot}1152$, $b = 0{\cdot}7994$ and $c = 1{\cdot}1492$ nm. The second major study was carried out by Coughanour, Roth, Marzullo & Sennett (1955) using powder XRD. They determined the room-temperature form of $CaZrO_3$ to be orthorhombic with lattice parameters $a = 0{\cdot}5587$, $b = 0{\cdot}8008$ and $c = 0{\cdot}5758$ nm. In addition, they mentioned that the $CaTiO_3$(and $CaZrO_3$)-type orthorhombic modification of ABO_3 compounds may not possess space group *Pcmn*, based upon their XRD intensity measurements. The most recent study is attributed to Koopmans, Van de Velde & Gellings (1983). They resorted to powder neutron diffraction for crystal structure and lattice-parameter determination of $CaZrO_3$ and $CaTiO_3$. They preferred the orthorhombic space group *Pcmn* over $Pc2_1a$ and *Amm*2, for both $CaZrO_3$ and $CaTiO_3$. The unit-cell parameters for $CaZrO_3$ were determined as:

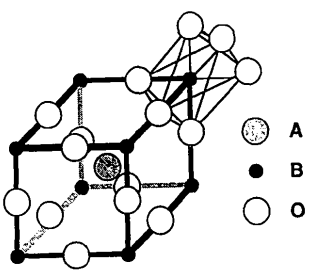

Fig. 1. Ideal perovskite structure of ABO_3-type compounds. Only one oxygen octahedron is emphasized.

0108-7681/89/030218-10$03.00